行政院國家科學委員會補助專題研究計畫成果報告

※※※※※※※※※※※※※※※※※※※※※※※※※
※　　　　　　　　　　　　　　　　　　　　　　　※
※　光資訊關鍵性材料製程與性質研究-總計畫(2/3)　※
※　　　　　　　　　　　　　　　　　　　　　　　※
※※※※※※※※※※※※※※※※※※※※※※※※※

計畫類別：□個別型計畫　　■整合型計畫
計畫編號：NSC92-2216-E-009-009
執行期間：2003 年 8 月 1 日至 2004 年 7 月 31 日

主持人：郭正次　國立交通大學 材料科學與工程學系
共同主持人：張立 謝宗雍 陳三元 吳耀銓 陳家富
計畫參與人員：林兆焄、陳柏林、王威翔、張志忠、林貞君、莊必愷、張峻愷、林奕同、邱國銘、林怡芬

本成果報告包括以下應繳交之附件：
□赴國外出差或研習心得報告一份
□赴大陸地區出差或研習心得報告一份
□出席國際學術會議心得報告及發表之論文各一份
□國際合作研究計畫國外研究報告書一份

執行單位：國立交通大學 材料科學與工程學系、機械工程學系

中　華　民　國　93　年　5　月　31　日

行政院國家科學委員會專題研究計畫期中進度報告

光資訊關鍵性材料製程與性質研究-總計畫(2/3)

執行期限：92 年 8 月 1 日至 93 年 7 月 31 日

計畫編號：NSC92-2216-E-009-009

主持人：郭正次　國立交通大學 材料科學與工程學系

共同主持人：張立 謝宗雍 陳三元 吳耀銓 陳家富

子計畫一：

碳基奈米結構材料之製程及其在場效顯示器上之應用

計畫編號：NSC92-2216-E-009-010

主持人：郭正次　國立交通大學 材料科學與工程學系

一、摘要

本研究藉由微波電漿輔助電子迴旋共振化學氣相沉積法(ECR-CVD)在陽極處理氧化鋁(AAO)模版的垂直孔洞中成功備製了高配向奈米碳管(CNTs)。本研究利用掃描式電子顯微鏡（SEM；scanning electron microscopy）和穿透式電子顯微鏡（TEM；transmission electron microscopy）分析奈米碳管的微結構。同時所得奈米碳管具有非常高的堆積密度和均勻的尺寸分布以及良好的石墨結構. 經由本實驗所得之 CNTs 的成長速率非常低，因此很容易經由調整合成的時間重製相同長度的 CNT。同時經由場發射的量測可以推論出本實驗所製作的 CNTs 具有場發射性質. 均一的尺寸分布、良好的配向以及良好的石墨特性。

關鍵詞：碳奈米管、石墨、微波電漿化學氣相沉積法、場發射

Abstract

Highly aligned carbon nanotubes (CNTs) have been successfully grown in vertical channels of the anodic aluminum oxide (AAO) template by microwave plasma electron cyclotron resonance chemical vapor deposition (ECR-CVD). Nanoporous AAO templates with hexagonal pore pattern were prepared by the two-step anodization of Al films. Following the electroplating of Co catalyst into the pore bottom, multiwalled CNTs were synthesized in the ECR-CVD system using a gas mixture of CH_4 and H_2. The microstructure of the CNTs was studied by scanning electron microscopy (SEM) and transmission electron microscopy (TEM). The CNTs with a very high packing density and a uniform size distribution are well-graphitized. The segments of CNTs stretching out of the AAO nanopores still maintain relatively good alignment, and have a very slow growth rate, which allows us to obtain reproducible tube length by tuning the growth time. Field emission measurements of the CNTs showed derivable electron emission properties, attributed to their uniformity in size, good alignment, and good graphitization properties.

Keywords: nanotubes, graphite, plasma CVD, field emission

二、計畫緣由與目的

在過去的幾十年間,奈米碳管(CNTs) 因為具有優秀的場發射特性，已經變成下一個世代冷陰極平面

面板顯示器以及真空微電子裝置最有潛力的材料之ㄧ[1-3]。當作電子發射材料必須具有需多特性，例如高的長寬比、小的曲率半徑、優良的化學穩定性以及高的熱穩定性和大的機械強度。然而，由於受限於上述的條件，因而諸多製程不相容於目前的半導體製程。對照上，同樣是電漿製程，冷電漿卻大量的使用在半導體製程中。故本研究計劃電子迴旋共振化學汽相沉積法(ECR-CVD)來合成碳基材料奈米結構。此方法不僅可直接沉積奈米結構於所選定的基材上(Si 晶片，或導電玻璃)，且可符合低溫的製程需求。亦將利用多孔氧化鋁做為奈米結構成長的模板來開發選擇性沉積製程技術。

三、結果與討論

圖 1a 顯示出兩步驟陽極氧化和孔洞擴大後的 AAO 薄膜奈米孔洞 SEM 上視影像。均勻尺寸分布的自組織奈米孔洞的直徑大約 60 ㎚， 而內部孔洞之間的距離約 100 nm。圖 1b 則是鈷觸媒電鍍前 AAO 薄膜的橫截面 SEM 影像。垂直的圓柱型孔洞深度大約是 740 ㎚，並且在每一個孔洞底部的絕緣氧化鋁障礙層經過擴孔的階段完全被移除。之後 Co 觸媒顆粒均勻被電鍍在 AAO 孔洞的底部 (如圖 1c).

Lee et al. [8] 曾經報導過不管有無觸媒在孔洞底部的AAO模板均可以生長 CNTs。但是 Co 對碳氫化合物分解，是具有非常高的活性 [9]，所以 Co 應該是最主要的催化者。圖 2 顯示出微波電漿 ECR-CVD 經 Co 觸媒催化 CNTs生長於AAO模板的SEM側視影像。同樣類似於先前的情形，CNTs 也會長出孔洞的外面，但是長出孔洞外面的奈米碳管整齊排列並垂直於 AAO 的表面，同時相互糾結在一起。圖 1 所示的是 CNT 的管徑大於 AAO 在 CNT 成長之前的奈米孔洞的直徑，這可能的原因是 AAO 模板經過 CVD 製程處理時，因為加熱造成水分散失，使得 AAO 的奈米孔洞孔徑變大，因此後來所成長的 CNTs 直徑會比原來 AAO 奈米孔洞的孔徑大。 [4].

從圖 2 可以看出 CNTs 的長度隨成長的時間增加而增加。圖 2a 所顯示的是，當 CNTs 成長 7 分鐘時大部分的 CNTs 都比 AAO 的奈米孔洞高度短，僅有少部分的 CNTs 長出 AAO 奈米孔洞之外；如果 CNT 成長的時間是 15 分鐘（如圖 2b 所示）則大部分的 CNT 都超過了 AAO 奈米孔洞，超過的長度大約是 300-700 ㎚；如果是 30 分鐘(如圖 2c 所示)大部份生成的碳管長度都超過模板 700nm 到 1.5 ㎛，但之後再增加 CNT 成長的時間，奈米碳管並未有再增加的趨勢，此時我們判斷 Co 觸媒已經遭到毒化。CNTs 製造三極體場發射器的主要挑戰是控制 CNTs 的長度、高配向和在次微米級裝置其長度不會超過閘極的孔深度[10]。由 ECR-CVD 在 AAO 模板內成長的 CNTs 成長速率相當低，大約是每分鐘 ~60 nm， 所以碳管的長度反而容易利用成長時間來控制，因此利用此法所生長的 CNTs 非常適合作場發射器的應用。

圖 3a 所顯示的是圖 2a 試片的 TEM 橫截面影像，從圖中可以很清楚看出來 Co 觸媒顆粒被封包在碳管的頂部，並且表面整個被石墨所覆蓋。雖

然殘存的 Co 觸媒顆粒也可能在碳管底部被觀察到，但是我們認為整個奈米碳管的成長機制傾向於 Tip growth 而不是 base growth。如果是 base growth 成長機制，碳氫化合物的前軀體必須連續不斷的傳遞到孔洞底部的 Co 觸媒進行催化反應成長 CNTs。但是在我們的實驗條件之下，每個奈米孔洞內部整個被多管壁奈米碳管完全填充。再者，每一根奈米碳管都僅有一個封閉端，同時 Co 奈米顆粒被封包在頂部也可能會阻塞住氣體的擴散，因此結果意味著 base growth 不是一個可能的成長機制。相反 tip growth 的成長機制，因為奈米碳管的成長位置是在碳管的頂端，所以氣體的擴散將不會被阻塞。

圖 3b 所顯示的是對圖 3a 上生長超出 AAO 孔洞外的 CNTs 所進行的一個選區電子繞射的圖形。由圖形中可以看出三個繞射環，經由鑑定它們所代表的分別是石墨的(002), (100), 和(110)的三個面。這些碳管具有一個石墨的結構，其內壁之間的距離 (d_{002}) 接近 3.6 Å，這比石墨 d_{002} 的值 (d_{002}=3.35 Å) 還大，可能是碳管管壁曲率的因素所造成。圖 3c 所顯示的是 CNT 在 AAO 模板孔洞內部的高解析度(HRTEM) 正視影像，此管大約有 70-80 個石墨層所組成，並且碳管管徑的大小被AAO孔洞的幾何形狀所限定住，值得注意的是石墨層的數目和成長時間無關；而且也不像是 Yao 等人[5]所提出的 layer-by-layer growth 的成長機制。從圖 2 上我們可以觀察出 Co 觸媒催化成長的 CNTs，成長時間增加的速度比 CNT 長度增加的速度快。 因此，我們認為在我們的實驗條件下 AAO 扮演觸媒的角色是遠低於 Co 觸媒的地位。

圖 4 所顯示的是，AAO 模板是基於三種不同合成生長時間的 CNT，其場發射電流密度和外加電場呈現一個函數關係。很明顯的合成時間 30 分鐘的 CNTs (超出 AAO 模板長度: 700 nm-1.5 μm) 出現最好的場發射性質比合成時間15 分鐘(超出AAO模板長度: 300-700 nm) 和 7 分鐘。合成時間 7 分鐘的電流密度最低 (< 3 $\mu A/cm^2$) 。圖 4 內的插圖是試片的 Fowler-Nordheim (FN)圖。圖中我們假設 CNT 的功函數是 5ev，而其斜率即是場強化因子 β。合成時間 30 分鐘和 15 分鐘的 β 值分別是 2600 和 1900。Suh[22]在他的實驗結論中發現當暴露在 AAO 模版外面的 CNTs 長度相當於 AAO 模板內部碳管之間的距離（大約 100 nm）時可以得到一個最佳的 β 值 (β ~ 2650) 。而我們實驗的碳管堆積密度是較低的 (CNT 填充 AAO 孔洞的比例 ~ 70%) 因此造成內部碳管之間的距離增加。最佳的場發射條件是從超過 AAO 模板 1 μm 長的 CNT 中得到。 為了避免造成場屏蔽效應[11]，反而是, 較低堆積密度的 CNTs 是比較好的。

四、計畫成果自評

本研究已經成功的藉由微波電漿輔助電子迴旋共振化學氣相沉積法在 AAO 模板內合成垂直排列的奈米碳管。其中 AAO 模版的效應和 DC 直流電偏壓以及電漿誘導自我偏壓對碳奈米管的垂直對準排列具有相當程度的影響。從本研究可以得到非常高堆積

密度的奈米碳管(超過 10^9 tubes/cm^2)以及較小的碳管直徑的分布(約 75 nm) 。本實驗所合成出來的 CNTs 是多管壁的 CNTs 有良好的石墨化 和場發射特性。因此非常有潛力應用在 冷陰極平板顯示器上。

五、參考文獻：

[1] S. Iijima, Nature 354 (1991) 56.

[2] Yahachi Saito and Sashiro Uemura, Carbon 38 (2000) 169.

[3] Niels de Jonge, Yann Lamy, Koen Schoots, and Tjerk H. Oosterkamp, Nature 420 (2002) 393.

[4] Jung Sang Suh and Jin Seung Lee, Appl. Phys. Lett. 75 (1999) 2047.

[5] B. D. Yao and N. Wang, J. Phys Chem. B 105 (2001) 11395.

[6] Po-Lin Chen, Cheng-Tzu Kuo, Tzeng-Guang Tsai, Bo-Wei Wu, Chiung-Chih Hsu, and Fu-Ming Pan, Appl. Phys. Lett. 82 (2003) 2796.

[7] Chao-Hsun Lin, Hui-Lin Chang, Ming-Her Tsai, and Cheng-Tzu Kuo, Diamond Relat. Mater. 11 (2002) 922.

[8] Jin Seung Lee, Geun Hoi Gu, Hoseong Kim, Kwang Seok Jeong, Jiwon Bae, and Jung Sang Suh, Chem. Mater. 13 (2001) 2387.

[9] Soo-Hwan Jeong, Hee-Young Hwang, Kun-Hong Lee, and Yongsoo Jeong, Appl. Phys. Lett. 78 (2001) 2052.

[10] Yun-Hi Lee, Yoon-Taek Jang, Dong-Ho Kim, Jin-Ho Ahn, and Byeong-kwon Ju, Adv. Mater. 13 (2001) 479.

[11] L. Nilsson, O. Groening, C. Emmenegger, O. Kuettel, E. Schaller, L. Schlapbach, H. Kind, J.-M. Bonard, and K. Kern, Appl. Phys. Lett. 76 (2000) 2071.

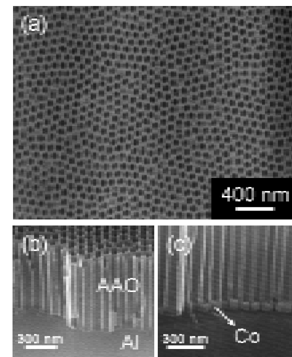

圖 1. (a) 奈米孔洞 AAO 薄膜的 SEM 上視影像。 (b) Co 觸媒電鍍前，AAO 薄膜的 SEM 截面影像； (c) Co 觸媒電鍍後，AAO 薄膜的 SEM 截面影像。

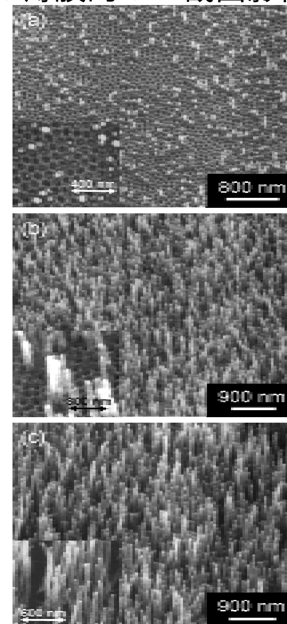

圖 2. 在 AAO 模板內 CNTs 的 SEM 側視圖影像，成長時間 (a) 7 min, (b) 15 min, 和 (c) 30 min。

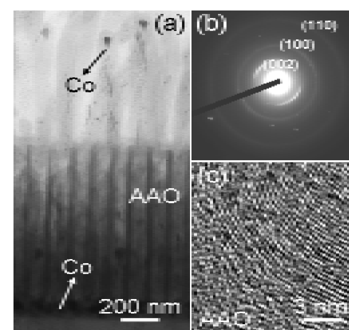

圖3.(a) 為圖2b試片橫截面的TEM影像。(b) 圖(a)生長超過 AAO 孔洞 CNTs 的電子繞射圖形.(c) 鑲嵌在AAO孔洞的CNTs之HRTEM 正視圖影像

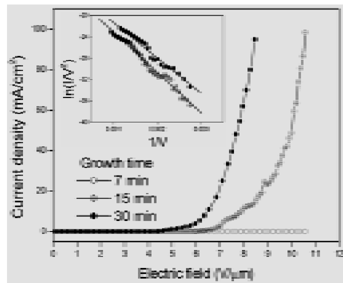

Fig. 4. 場發射電流密度vs. CNTs生長時AAO奈米孔洞之電場強度.

子計畫二：
各種型態之奈米碳基材料開發及場發射元件之製作(2/3)

計畫編號：NSC 92-2216-E-009-007
執行期限：92 年 8 月 1 日至 93 年 7 月 31 日

主持人：陳家富　　　　國立交通大學 材料科學與工程學系
計畫參與人員：林建良、徐振航、詹適宇、伍泰霖
國立交通大學 材料科學與工程學系

摘要

Material with high aspect ratio is essential for the typical field emission application. In this report, nano materials are synthesized and characterized using different techniques.

By using microwave plasma chemical vapor deposition system, Si nanotips are locally formed by an etching process. The microstructures of the Si tips are observed using both transmission electron microscopy and scanning electron microscopy. Further treatment is introduced to modify the tip structure to enhance the field emission properties comparative to the Si tips. With the similar technique, chromium carbide capped carbon nanotips are synthesized. This material also performs good uniformity and field emission properties. Proposed growth mechanism is demonstrate to provide a possible route to synthesized different catalyst cap on the tip in order to tune the field emission property.

Aluminum nitride nanotips are synthesized using thermal chemical vapor deposition. AlN nanotip appears in hexagonal shape and high resolution TEM shows a perfect crystalline structure. By controlling the cluster size and the growth temperature, the desired microstructure can be formed.

計畫緣由與目的

With the development of nanotechnology, nanostructures-structures that are defined as having at least one dimension between 1 and 100 nm have received steadily growing interest as a result of their peculiar and fascinating properties, and applications superior to their bulk counterparts. Many applications are predicted to involve with nanotechnology including optics, electronics, catalyst, ceramics, and storage media, etc. The most pertinent example is microelectronics, which “smaller” means greater performance ever since the invention of integrate circuits: more components per chip, faster operation, lower cost, and less power consumption.

Field emission from nano-sized material is one of the most important applications for the nanotechnology. The basic requirement of a nano emitter must have a high aspect ratio that field emission will take place. Among such an application, a revolution of the display technology come the field emission display. Compare with TFT-LCD flat panel display, field emission display has much more advantages such as high brightness, thin in dimension, wide view angle, low power consumption and a wide operating temperature. The mention advantages above make the field emission display a candidate for the new generation of the display technology.

Though the field emission technology has been developed over decades, a satisfied product has not yet been demonstrated. The key resolution of the current field emission display difficulties is the field emission efficiency and durability of the emitters. So far, carbon nanotubes have been extensively studied and tested for applications. It is not until now that precisely controlling the dimension and

distribution of carbon nanotubes still a challenging issue. There's still many materials which prohibit better performances than carbon nanotubes do.

In this project, various kinds of deposition methods are involved to synthesized nano-size materials. After the synthesis, instruments are incorporated to analysis and measure the character of the material. At the final stage, the material with desirable performance will be fabricated in to the device to achieve the practical applications.

結果與討論

A. Modification of Si Nano Emitters by Diamond - clad Process

The potential to achieve high-current devices is one of the most attractive issues of field emitters. In this work, needle-like Si tips with high aspect ratio is achieved by hydrogen plasma. Scanning electron microscopy (SEM) shows the average diameter and height of need-like Si tips are approximately 70 and 350 nm, respectively. To improve the field emission property of pure Si tips, the diamond-like carbon nanoparticles are further deposited on the top of the Si tips. Experimental results present that the diamond-like carbon-clad process improves the stability as well as the conductivity. Transmission electron microscopy (TEM) and Raman spectroscopy are used to observe their nanostructures and quality. Besides, the Auger electron spectrum also detects the partial growth of silicon carbide during modification process.

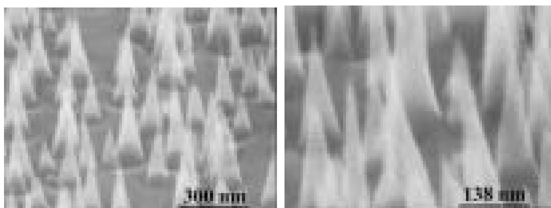

Fig. 1 (a) High and (b) low magnification of SEM photographs of Si nanotips

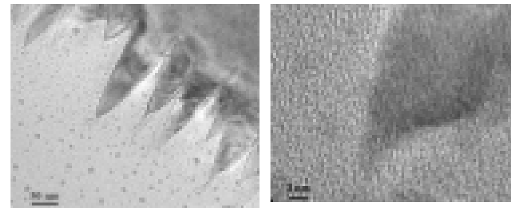
Fig. 2 TEM of (a) Si tips and (b) high-resolution images of individual Si tip.

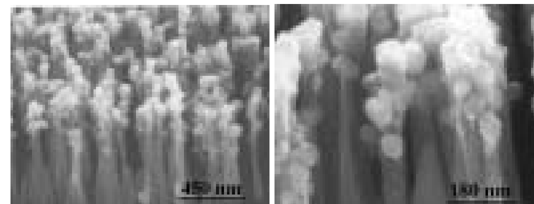
Fig. 3 (a) High and (b) low magnification of SEM photographs of DLC-clad Si nanotips.

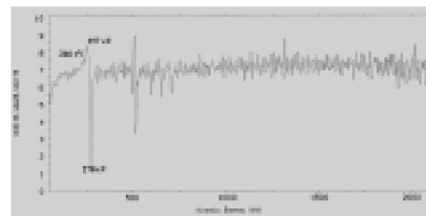
Fig. 4 AES profile of DLC-clad Si tips.

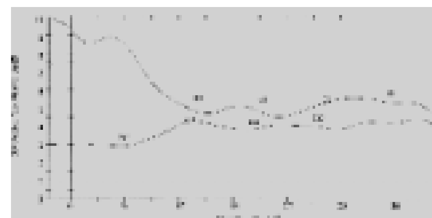
Fig. 5 AES surface survey of DLC-clad Si tips.

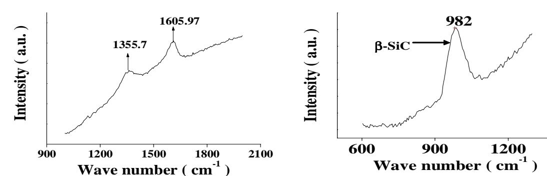

Fig. 6 Raman spectrum of DLC-clad Si nanotips.

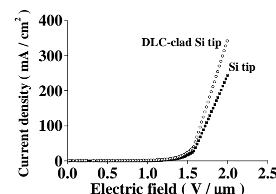

Fig. 7 Electric field (E) versus current density (J) of Si and DLC-clad Si tips, respectively.

According to the mentioned results, the major findings are summarized as follows:

1. The application of hydrogen plasma to induce Si tips is an easy method to

produce high aspect ratio field emitters in many systems.

2. The average diameter and height of needle-like Si tips are approximately 70 and 350 nm, respectively.
3. Due to the competition between deposition and etching rate simultaneously occurred in the plasma, the needle-like shaped of Si tips becomes blunt after DLC deposition.
4. Negative-bias effect is expected to enhance the growth rate of DLC during deposition.
5. Improvement on I-V characteristic of DLC-clad Si tips is due to the negative electron affinity (NEA) property and carbon nanoparticles.

B. Growth of chromium carbide capped-carbon nanotip using bias-assisted microwave plasma chemical vapor deposition

Chromium carbide capped-carbon nanotip was synthesized using bias-assisted microwave plasma chemical vapor deposition. Such a material grew up to about several hundreds of nanometer long and tens of nanometer in diameter. The applied bias is a significant parameter in the growth process that the higher bias is effective to increase the growth rate. However, the higher bias also contributes to a rapid formation of chromium carbide which leads to a shorter length of carbon nanotip at the same time. The higher ion energy also varies the tip diameter due to strong ion bombardment effect which is a competitor to deposition. It is found that the growth of chromium carbide capped-carbon nanotips reaches a limit due to the fully carburization of chromium.

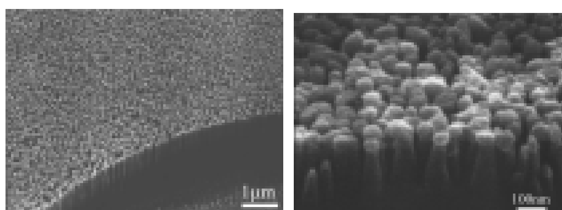

Fig. 1 (a) Low magnification SEM image showing the uniformity of the vertical aligned chromium carbide capped carbon nanotips. (b) SEM image of a close view.

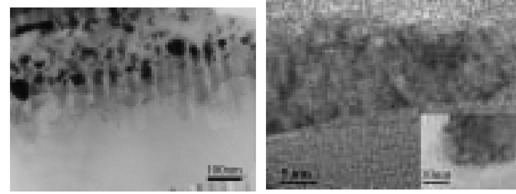

Fig. 2 TEM images showing (a) the cross-section view of chromium carbide capped carbon nanotips and, (b) high magnification view of an individual carbon nanotip and the inset shows the chromium carbide head.

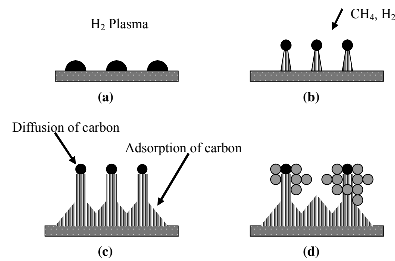

Fig. 3 Schematic diagram of proposed growth model (a) Formation of nucleation process; (b) cap growth; (c) deposition of carbon (d) asparagus-like structure forms.

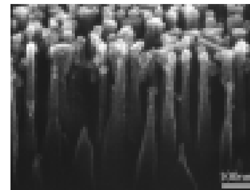

Fig. 4 Chromium carbide capped carbon nanotip grew under bias of -300 volt for 30 minutes

Chromium can be used as a catalyst to grow chromium carbide capped carbon nanotip with size of several tens of nanometers. Surface diffusion is believed to be the mechanism for the growth of carbon nanotip. The applied bias plays an important role that either assists the growth or etches the carbon away during growth. In other words, the dimension of the chromium carbide capped carbon nanotip can be controlled. And there exits length limit which is due to the fully carburization of chromium. By supplying sufficient bias, an asparagus–like structure forms.

C. Nucleation and growth of aluminum nitride nanotips using chemical vapor deposition

Hexagonal aluminium nitride nanotips

(AlNNTs) have been fabricated on silicon (Si) substrates by simply using thermal chemical vapor deposition at temperatures of 950°C, using aluminium (Al) powders and ammonia gas. The initial growth of AlNNTs reveal that metal- silicide nanoclusters formed during early stages of growth served as the nucleation sites for the nanotips growth. Size control can be achieved by controlling the thickness of metal catalyst deposited on the silicon substrate. A stable and self-limited (001) facet often inhibits further growth of the AlNNTs grown at high temperatures. The area of the (001) facet increases with the increasing growth temperature. The structure and chemical composition of the AlNNTs were investigated by using XRD analysis, high-resolution electron microscopy, electron energy loss spectroscopy, and elemental mapping.

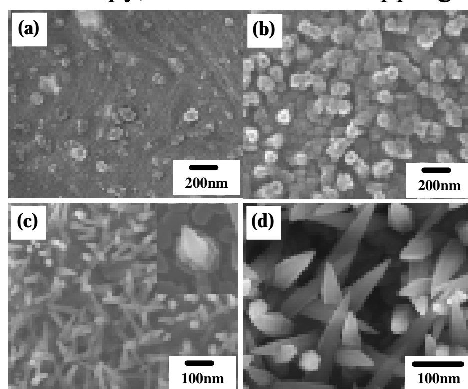

Fig.1. High resolution scanning electron microscope images of AlN nanotip grown for (a) 15 min, (b) 20 min, (c) 25 min, Inset shows the high magnificent of the initial growth of nanotip with crystalline nanoparticle on the base of the AlNNTs. (d) 30 min, respectively.

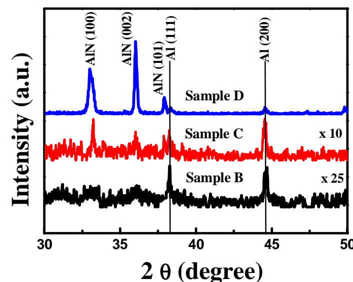

Fig.2. XRD spectra take from the sample B, C, and D, respectively.

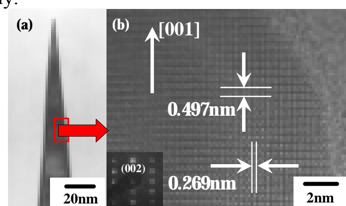

Fig. 3. (a) Low magnification HRTEM image and (b) atomic resolution TEM image of the h-AlN nanotip with growth direction of [001] with [110] zone axis. Inset in (b) shows SAED image of the AlN nanotips.

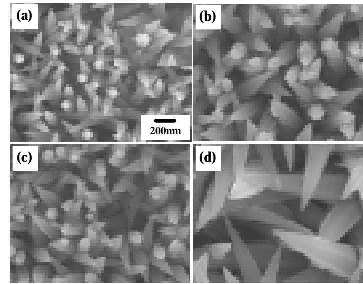

Fig.4. HR-SEM images of AlN nanotips grown with (a) Au (15nm), (b) Al (15nm), (c) Pt(15nm), (d) Pt (60nm) coating on the Si substrate, respectively.

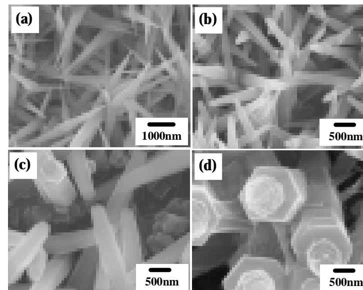

Fig.5. HR-SEM images of AlN nanotips on silicon substrates coated with 15 nm of gold grown under (a) 950°C, (b) 1000°C, (c) 1100°C, (d) 1200°C, respectively.

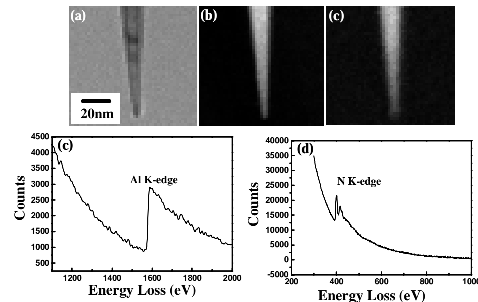

Fig. 6. EELS experiments and elemental mapping of the AlN nanotips: (a) Original TEM image; (b) Al mapping; (c) N mapping. Corresponding EELS spectra exhibiting (d) Al K-edge at 1560 eV, (e) N K-edge at 401eV. All the EELS analysis were obtained from AlN nanotip(s) prepared on 15 nm Au coated Si substrate at 950°C for 30 minutes.

In summary, the growth of highly pure and high density hexagonal aluminum nitride nanotips on silicon substrates via a thermal chemical vapor deposition system has been demonstrated. The AlNNTs grow by vapour-solid mechanism and their preferred growth direction (long axis) is [001]. Composition and structures of the AlNNTs have been confirmed by XRD, HRTEM, SAED, and EELS. Optimal conditions for the growth of these nanotips are 950°C growth temperature

and 30 minutes growth time under flowing NH_3 with Au as catalyst. The morphology of the nanotips is determined by the size of the metal or metal silicide phase nanoparticulates formed during the initial stages of growth. It is believed that this nanotip structure have potential applications as field emission tips, and other nanoscale heterojunction devices.

計畫成果自評

本計畫成功的利用多種方法合成各種型態的奈米材料,包括奈米碳管、奈米矽尖錐、奈米碳尖錐及奈米氮化鋁尖錐。

在直接利用矽晶圓的情況下，藉由偏壓輔助微波電漿化學氣相沈積法，可蝕刻形成矽的奈米尖錐，更可再藉由後處理披覆類鑽薄膜以增進其場發射性質。此法可望直接利用現有半導體製程以製作元件。另外直接利用觸媒成長法選擇性成長奈米碳尖錐及奈米氮化鋁尖錐，皆具有優良的性質。並深入研究其成長特性進而控制奈米材料的外型及組成。

除了可以直接應用於場發射元件上，這些一維的奈米材料因具有極高的表面積，可應用在需高表面積反應的需求上，例如燃料電池、氣體偵測器及生化感測器上。除此之外，這些奈米材料仍待更進一步的開發與應用。

子計畫三：

奈米結構氧化物光子晶體材料製程與光電特性研究(2/3)

Growth kinetics and microstructure evolution of well-aligned and patterned ZnO nanorods on **Si-based substrate in aqueous solution**

計畫編號：NSC92-2216-E-009-014

執行時間：92/08/01 ~ 93/07/31

主持人：陳三元 教授　　　　交通大學材料科學與工程學系

中文摘要

在低溫下合成單晶 ZnO 奈米線的成長動力學和微結構的發展已經研究完成。在不同特性基版上的 ZnO 奈米線會表現出不同的成長行為和方向。在純 Si 基版上，ZnO 奈米線會散亂地沿著(100)優選平面或 $[01\bar{1}0]$成長方向，排列在整個基版上。由高解析穿透式電子顯微鏡(HRTEM)觀查可得到，散亂的 ZnO 奈米線其實是自我組裝的兩階段式成長所得到。相對的，如在是在 ZnO film/Si 的基版上，規則排列的 ZnO 奈米線是直接從 ZnO film 上沿著[0002]方向成長。相比散亂的 ZnO 奈米線，規則排列的 ZnO 奈米線，有大的長寬比，可以到 25 到 30。另外，有一些平面缺陷，例如疊差(stacking faults)產生是由於 ZnO 成長單元在後期快速成長的結果。這些結果與發現暗示著，從溶液成長的規則排列 ZnO 奈米線不是直接跟基版有關，而是跟基版的表面的凹凸率直接相關。

Abstract

Growth kinetics and microstructure evolution of single-crystal ZnO nanorods (ZNs) synthesized in aqueous solutions at low temperatures were investigated. Depending on surface characteristics of substrate, ZNs present different growth behavior and direction. On pure Si substrate, ZNs were scattered over the entire Si substrate with a preferred orientation in the (100) plane or grown along $[01\bar{1}0]$ direction. HRTEM observation demonstrates that the scattered ZNs present two-stage growth process with a self-assembly process of ZNs in the later growth stage. In contrast, on Si wafer with ZnO film coated, well-aligned ZNs were directly grown along [0002] direction from the ZnO film on Si. In comparison with the scattered ZNs, a larger aspect ratio (length/width) up to 25-30 was obtained for the well-aligned ZNs. In addition, some planar defects such as stacking faults were probably resulted due to faster growth of ZnO growth unit in the later growth stage. These observations and findings imply that the growth of the well-aligned ZNs from the soft solution is not related to the used substrates but strongly influenced by the surface characteristics as well as roughness of the substrate.

I. Introduction

One-dimensional (1D) nanostructures have great potential for learning the fundamental concepts of the roles of both dimensionality and size in physical properties as well as for application in nanodevices and functional materials. Other than carbon nanotubes, 1D nanostructures such as nanowires are ideal systems for investigating the dependence of electrical transport, optical and mechanical properties on size and dimensionality.[1]

Zinc oxide (ZnO) is an important electronic and photonic material because of its wide and direct band gap (ΔEg = 3.37eV) material.[2] The strong exciton binding energy of ZnO (60meV) is much larger than that of GaN (~ 25meV), which can ensure an efficient exciton emission at room temperature.[2] Recently, highly oriented nanorod array of ZnO nanostructures have demonstrated their potential applications in manufacturing electronic and optoelectronic devices.[3-5]

Various methods including chemical, electrochemical, and physical deposition techniques have been employed to synthesize 1D ZnO nanostructures such as catalytic growth via the vapor-liquid-solid (VSL) epitaxial method[6] and metal-organic-chemical vapor deposition (MOCVD).[7-8] However, those methods are expensive and energy consuming processes since they are operated under extreme conditions. It is well conceived that preparation of ZnO via solution chemical routes provides a promising option for large-scale production of this materials. Although wet-chemical approaches have been used for large oriented arrays of ZnO nanorods on polycrystalline (or single-crystalline) substrates from aqueous solutions[9-10], it is worth noting that without suitable treatment on the substrate, highly oriented ZnO nanorods grown on a Si wafer has been rarely achieved due to the larger mismatich (~40%) between the substrate and the ZnO nanorods.

Yamabi *et al.* reported that without undercoats on the surface, clusters of spindle-shaped hexagonal crystallite with diameters of 0.5-1.0 um were scattered over the surface of a silicon wafer, but highly aligned arrays of ZnO nanorods with diameters of 20-100 nm can be developed on Si substrate undercoated with $Zn(Ac)_2$ and annealed at 500°C.[10] Recently, Choy *et al.* also found that high-quality ZnO nanorods were successfully grown on a Si wafer by a wet-chemical process at 95°C for 6 h, where the Si wafer was dip-coated with 4 nm sized ZnO nanoparticles as a buffer and seed layer prior to crystal growth.[11] These observations reveal the importance of surface characteristics or treatment in the growth of well-oriented ZnO nanorods in aqueous solution. However, little investigation was paid attention to the growth behavior and kinetics of such ZnO nanorods, in particular to tailor their orientation onto the substrates, that can be used to control the structure morphology and optoelectronic properties.

Therefore, in this work, a simple wet-chemical method was used to study the growth kinetic of both scattered and aligned ZnO nanorods on Si by monitoring the average aspect ratio of ZnO nanorods as a function as growth time in aqueous solution. By controlling the experimental conditions, well-aligned arrays of ZnO nanorods with different aspect ratios can be obtained. Moreover, high-resolution transmission electron microscopy (HRTEM) was performed to investigate the growth mechanisms of ZnO nanorods.

II. Experimental

Zinc nitrate hexahydrate ($Zn(NO_3)_2 \cdot 6H_2O$) was used as the Zinc precursors to synthesize the ZnO nanorods (ZNs). Methenamine ($C_6H_{12}N_4$), also called hexamethylenetetramine (HMT) is a highly water soluble, non-ionic tetradentate cyclic tertiary amine and used to comply

simultaneously with the precipitation of the divalent post-transition metal Zn^{2+} ions, the nucleation growth of its stable oxide form, zincite ZnO. Two kinds of substrates were also used for comparison in this study. One is Si and the other is Si coated with ZnO film. The ZnO thin films were deposited on Si substrates by rf magnetron sputtering following our previous report.[12] An equimolar (0.02M) aqueous solution of $Zn(NO_3)_2 \cdot 6H_2O$ and HMT was prepared in a bottle. Subsequently, substrates were placed inside the aqueous solutions and heated at ambient temperature (55-95^oC) for 0.1-15 h. After that, the substrates were removed from the aqueous solutions, rinsed with distilled water, and dried at room temperature overnight.

X-ray diffractometer (M18XHF, MAC Science, Tokyo, Japan) was used to examine the crystalline phase of the synthesized compounds with a scanning rate 4° (2θ) per min over a 2θ range 20- 60°. The morphology of the ZnO nanorods was examined by scanning electron microscopy (SEM, Hitachi model S4000). Microstructure observation was performed by transmission electron microscopy (TEM) with a Philips Tecnai 20 instrument (Holland, The Nertherlands), operated at 200 keV. A double-tilt specimen holder was used to tilt several zone-axes. High-resolution images were recorded at several exact zone-axes with Scherzer defocus at –67nm and at an electron-optical magnification of 490000 to 520000.

III. Results and discussion

3.1 Phase and morphology of ZnO nanorods grown on different substrates

Two substrates, i.e., Si and ZnO-coated Si, were used in this work to study the growth behavior of ZnO nanorods (ZNs) in the precursor solution at different temperatures of 55-95^oC for several hours. No ZNs were observed below 50^oC, indicating a thermal barrier for the growth of ZNs can not be overcome. Above 95^oC, ZNs can not be synthesized because the reaction temperature is near to its melting point of the aqueous solution. Figure 1 shows the SEM images of the as-synthesized ZNs grown on these two kinds of substrates at 75^oC for 10 h in the 0.02M solution. As shown in Fig. 1(a), ZNs with the dimension of 7-10 μm in length and 0.5-1 μm in diameter were scattered on the Si substrate. On the other hand, high density of well-aligned ZNs with dimensions of 20-200 nm in diameter and up to several μm in length were obtained uniformly when ZNs were grown on ZnO_f/Si as shown in Fig. 1(b). It seems to imply that the formation of well-aligned ZNs on a pure Si substrate is difficult because a large mismatch (~40%) exists between ZnO and Si. Based on this reason, this would retard the nucleation of ZnO on Si substrate. Consequently, it strongly reveals the importance of the substrate characterization on the growth behavior of ZNs in the aqueous solution.

The X-ray diffraction patterns (XRD) show that the ZnO crystal phase starts to appear at 50^oC and well crystallized above 65^oC. As shown in Fig. 2(a) and (b), a strongly oriented peak can be indexed as the wurtzite ZnO at 75^oC in 0.02 M aqueous solutions for the ZNs grown on Si and ZnO_f/Si substrate. However, it should be pointed out that a remarkable difference in XRD patterns exists between those two

substrates. As shown in Fig. 1(a), the diffraction peaks were indexed as (100), (002) and (101) planes of ZnO for the ZNs grown on Si substrate. On the other hand, Fig. 2(b) illustrates that the strongest diffraction peak corresponding to the (002) plane of ZnO was detected when the ZNs were grown on ZnO_f/Si substrate. These observations obviously imply different growth behavior between (100)-oriented (called as scattered) ZNs on Si and (002)-oriented (called as aligned) ZNs on ZnO_f/Si.

3.2. Microstructural analysis of ZnO nanorods

It is well known that ZnO has as a hexagonal lattice with c/a axial ratio of 1.602.[13] The most commonly observed morphologies of ZnO are either rod-like or needle-like crystals, especially prepared ZnO in aqueous solution because of anisotropic crystal growth. The transmission electron microscopy (TEM) bright-field (BF) image and corresponding selected-area diffraction (SAD) pattern of the scattered ZNs are shown in Fig. 3(a) and (b), respectively. The SADP in Fig. 3(b) clearly indicates that the scattered ZNs were grown along $[01\bar{1}0]$ direction. This result is also inconsistence with the XRD analysis that the ZNs are preferentially oriented along $[01\bar{1}0]$ direction. A close examination of the SADP in Fig. 3(b) shows the split of diffraction spots and extra diffraction spots, located at halfway between the central (000) spot, the {0002} spots and $\{01\bar{1}0\}$ spots. However, no Morié fringes were observed in the corresponding High-resolution TEM (HRTEM) in Fig. 3(c) so that double diffraction can be neglected in this study.

Since the crystallographic phase of these ZNs belongs to wurtzite structure with a space group of $P6_3mc$, it easily appears as a characteristic "zigzag" structure,[14-15] so-called "superlattice diffraction", corresponding to the observed extra spots in the SADP. It seems to imply that the crystal structure of the scattered ZNs was constituted from many tiny areas such as domains or mosaic texture according to the disoriented few degrees in SADP. It is well known that a crystal with mosaic structure does not have its atoms arranged on a perfectly regular lattice extending from one side of the crystal to the other; instead, the lattice is broken up into a number of tiny blocks, each slightly disoriented one from another. Within these tiny blocks, there exists a structural mismatch at the interface between these domains.[16] This mismatch may be very small and involve a difference in angular orientation between the domains as in our case with 1~2° difference in the SADP. Furthermore, HRTEM image in Fig. 3(c) recorded from this scattered ZN reveals that there seem to be two types of lattice fringes in this HRTEM image: one with wave-like fringes (as arrowed in Fig. 3(c)) and the other with straight fringes. This variation of lattice fringes as marked with arrows seems to be caused by these two types of crystal arrangements.

Figure 4(a) shows the TEM bright-field (BF) image of the aligned ZNs grown on ZnO_f/Si substrate. In contrast to the scattered ZNs, most of the ZNs were grown in a direction perpendicular to the ZnO_f/Si substrate. 4(b). A higher magnification in Fig. 4(b) indicates that the lattice fringes are

perpendicular to the longitude direction of the ZNs, and the singular fringe spacing is about 0.51nm, which is nearly consistent with the *c*-axis parameter in hexagonal ZnO structure (*c*= 0.521nm in ZnO structure). This demonstrates that [0002] direction is the preferred growth direction for the well-aligned ZNs. In addition, as one pays attention to the interface between ZNs and ZnO_f/Si shown in Fig. 4(c), it was observed that the well-aligned ZNs seem to be grown from the cup tip near the grain boundary between two ZnO grains in ZnO film. The formation of the cup shape around grain boundary between two ZnO grains is supposed to be correlated with the solution reaction during the nucleation and growth of ZNs. This demonstrates that the cup tip probably becomes a preferential nucleation position for the well-aligned ZNs grown on ZnO_f/Si. However, in addition to (0002) fringes, some ZNs with white lines dissecting the ZNs can be occasionally identified as marked with arrows in Fig. 5. This kind of planar defects can be considered as extrinsic stacking faults with insertion of an extra Zn-O layer parallel to the basal plane. It was worth noting that the presence of (0001) stacking faults provides a possible diffusion path to modify its optoelectronic properties according to our study. [17] However, well-aligned ZnO nanorods without any planar defects can be also obtained in aqueous solution by controlling the experimental conditions.

3.3 Growth behavior and kinetics of ZnO nanorods

It is well known that the growth behavior of ZNs was strongly influenced by the growth conditions such as ion concentration in solutions, reaction temperature and time. As illustrated in Fig. 6, the aspect ratios (AR =length/width) of ZNs grown on Si and ZnO_f/Si substrate as a function of growth time at 75°C were measured.

When the Si substrate without ZnO film coated was placed in the Zn-containing aqueous solution, in the initial growth stage of ZNs, prior to 0.2h, no obvious ZNs can be detected. However, above that (0.2-0.3h), it can be observed that a small amount of ZNs with ~20 nm in diameter and ~60 nm in length were randomly scattered on Si substrate according to SEM images (not shown here). However, at the same period of growth time, no any well-aligned ZNs can be clearly observed from the Si substrate. It seems to imply that the formation of well-aligned ZNs on a Si substrate is difficult based on the lattice parameters of ZnO and Si because a large mismatch (~40%) exists between ZnO and Si and this would retard the nucleation of ZnO on Si substrate. This phenomenon reveals that the well-aligned ZNs remain in the nucleation stage, but the scattered ZNs are going through nucleation and growth stage. Until 0.5 h, the well-aligned ZNs can be clearly obtained but the scattered ZNs have been grown with an AR of 2-3. Subsequently, with an increase of growth time, it can be observed that the increasing rate of the AR becomes slower in the scattered ZNs as compared to that in the well-aligned ZNs. Especially, above 5 h, the AR for the scattered ZNs remain unchanged with a constant of about 9-11 but the AR is also slightly decreased with increasing growth time up to 15 h. This implies that the

scattered ZNs did not further grow as expected despite extending growth time. As evidenced from the TEM BF image and corresponding SADP of ZNs grown for 5 h in Fig. 7, it seems to indicate that more than two ZNs with the same [01$\bar{1}$0] growth direction were self-assembled together to form a bundle. The TEM dark-field (DF) image clearly reveals that more than two ZNs were aggregated in a coplanar manner using their side planes to form a large ZN as shown in Fig. 7(c). This bundle ZNs can be further transformed into another ZN with a larger dimension in diameter. In other words, the side crystal planes of the ZNs were able to glue together to form a larger crystal. This behavior is also called "oriented attachment".[18] Based on viewpoint of thermodynamic, this self-assembling process is possible for the synthesized ZNs to reduce total Gibbs free energy in the later growth stage. This phenomenon is very similar to the Ostwald ripening occurring in ceramic sintering progress. This observation may be used to explain the slight decrease in AR in the later growth stage (5 -15 h). Consequently, the growth behavior of the scattered ZNs can be considered as a two-step growth mechanism.

In contrast, as the ZnO_f/Si substrate was used and immersed into the precursor solution for the growth of ZNs, it was found that in the early stage ($t < 0.5$), no aligned ZNs can not be clearly observed from the ZnO_f/Si substrates but at $t = 1$ h, a smaller AR was obtained for the well-aligned ZNs compared to that of scattered ZNs. It was believed that the ZnO nuclei will be preferentially grown on the ZnO_f/Si substrate in this stage and the promotion of heterogeneous nucleation is ascribed to the high affinity of the nuclei of ZnO for the surface, especially formed at the cup sites as shown in Fig. 4(c). In this condition, although an inherent asymmetry along the c axis allows the anisotropic growth of the crystal along the [0002] direction, the lateral growth along different directions are possible for the nucleus to decrease the roughness of the film surface because of surface energy effect. When the favorable nucleation position of ZN was formed on the ZnO film, ZnO growth unit (or called coordination polyhedron) will stack in order and grow along [0002] direction. Subsequently, a fast growth along longitudinal direction (c-axis) for the well-aligned ZNs was expected because the growth in width direction is suppressed due to the size of cup shape in ZnO_f/Si substrate. In 15 h, well-aligned and highly oriented ZNs with an aspect ratio up to 25-30 can be obtained. These results can be used to explain the observation that the well-aligned ZNs with a smaller AR were formed in an early stage but later, the ZNs were rapidly grown along the longitudinal direction in the later growth stage. Therefore, in this condition, some stacking faults are accidentally observed as shown in Fig. 5 that is probably due to faster stacking and the instability of the polar (002) plane in ZnO.

3.4

Figure 1a shows the surface images of large-scale arrayed ZnO nanorods grown on polystyrene (PS)/polycarbonate (PC) substrates. It was found that the ZnO nanorods have a well-defined hexagonal plane with a homogeneous diameter of

approximately ~60 nm due to uniform growth rate. The cross-section image in Figure 1b shows that the ZnO nanorods with a uniform length of 1.5 μm are directionally and densely grown over the entire PS surface of the substrates. Furthermore, we found that the patterned ZnO nanorods (Fig. 1c) can be developed after the removal of the PS beads in the specimen produced by the same conditions as Fig 1b. It implies that the PS layers can act as a nucleation base to supply the appropriate environment to increase the probability of the high density of nucleation sites and enhance the crystal growth.

To understand how the well-aligned arrays of oriented ZnO nanorods were formed on the organic substrates, the sample was further investigated by SEM and TEM. Three stages can be identified for the growth of ZnO nanorods on PS layers. The first initial stage ($t < 0.5$ h) is the induction time, during which an ultra-thin monolayer was slowly generated under the surface of PS beads in the solution. It is difficultly observed by SEM microscopy but the ultra-thin monolayer can be simply detected to be ZnO signal by chemical analysis such as X-ray photon spectroscopy (not shown) after removing the PS beads. The second stage is the nucleation period, during which the concentration of the building units in the solution builds up until a critical super-saturation level is reached and then nucleation occurs (Fig. 2a). It was believed that the ZnO nuclei will be preferentially grown on the concave regions of PS layers in this stage and the promotion of heterogeneous nucleation is ascribed to the high affinity of the ZnO nuclei to the PS surface. After nucleation, in the third period, a fast growth along longitudinal direction (c-axis) for the oriented ZnO nanorods was expected because the growth in width direction is suppressed due to the size of concave shape in PS layers as shown in Fig. 2b. Figure 2c shows the high resolution TEM (HRTEM) image of the well-aligned ZnO nanorods grown on PS/PC substrates. It indicates that the lattice fringes are perpendicular to the longitude direction of the ZnO nanorods, and the singular fringe spacing is about 0.51nm, which is nearly consistent with the *c*-axis parameter in hexagonal ZnO structure (c= 0.521nm in Wurtzite ZnO). This demonstrates that <001> direction is the preferred growth direction for the well-aligned ZnO nanorods. Recently, it was reported the aligned ZnO nanorods can be grown on the Si substrates with ZnO buffered layers which consists of nanoparticles or crystalline films.[16,17] However, most reports in the literature ignored the effect of surface morphology on the nucleation base of the aligned ZnO nanorods. Therefore, a HRTEM analysis was paid attention to the interface between ZnO nanorods and ZnO monolayer (~5 nm thicker) shown in Fig. 2d after removing the PS beads. It was observed that the well-aligned ZnO nanorods seem to be grown from the concave tip near the grain boundary between two ZnO grains in ZnO monolayer. A detail investigation for the growth behavior and kinetics of ZnO nanorods grown on inorganic substrates were reported in our previous study.[19] This demonstrates that the well-aligned ZnO nanorods can be grown on organic and inorganic substrates with controlled surface

morphology.

Figure 3a presents the SEM surface image of ZnO nanorods grown on organic substrates more than 24h. It was found that the ZnO nanorods begin to amalgamate with other neighboring nanorods and their growth becomes physically limited. In comparison with Fig. 1a, the ZnO rods become much thicker (more than 0.5 μm) but not much longer (about 1.7 μm) after long-term growth because the ZnO nanorods have started on coalescence process with adjacent rods. Therefore, after the lateral growth begins, the growth rate of ZnO nanorods in the <001> orientation would obviously decrease. The TEM bright-field (BF) image (inset in Figure 3a) of the <001> zone-axis of (cross-sectional) ZnO nanorods clearly illustrated the merged grains with side crystal plane attached. Moreover, as confirmed by Figure 3b for the <001> zone-axis selected-area electron diffraction (SAED) pattern of ZnO nanorods. The split diffraction spots in the edge region (marked with arrows) of the SAED pattern suggest that the merged ZnO nanords are not perfectly aligned in both *a* and *b* directions. The longitudinal direction is along the *c* <001> orientation. The TEM images in Fig. 3c and d reveal the BF and dark-field (DF) images of the merged ZnO nanorods, respectively. The DF image in Fig. 3d clearly and visibly shows that more than two ZnO nanorods were aggregated in a coplanar manner using their side planes to form a larger ZnO nanorod. A magnified picture of Fig. 3c was illustrated in Fig. 3e. The insets in the left and right of Figure 3e present the SAED patterns of single and couple nanorods in coalescent ZnO nanorods, respectively. The split diffraction spots were also identified from the couple rods and a slight misalignment between nanorods was observed. The growth behavior of the larger ZnO nanorods in later long-term growth can be considered from direct combination of a small number of individual nanorods which was similar to oriented attachment.[2]

IV. Conclusion

We have developed a low-temperature synthetic route to prepare well-aligned arrays of oriented ZnO nanorods with high crystallinity in the diameter of ~60 nm on the Si substrates. Single-crystal ZnO nanorods (ZNs) can be synthesized in an aqueous solution at 75°C. Depending on the surface characteristics of the substrate, ZNs present different growth behavior and direction. On pure Si substrate, ZNs were scattered over the entire Si substrate with a preferred orientation in the (100) plane or grown along $[01\bar{1}0]$ direction. HRTEM observation demonstrates that the scattered ZNs present two-stage growth process with a self-assembly process of ZNs in the later growth stage. In contrast, on Si wafer with ZnO film coated, well-aligned ZNs were directly grown along [0002] direction from the ZnO film on Si. In comparison with the AR of the scattered ZNs, a larger AR up to 25-30 was obtained. Although the surface characteristics of the substrates plays a very important role in both scattered and well-aligned growth of the ZNs, the ZnO film on Si wafer is surely to reduce the mismatch between the Si substrate and the ZnO nanorods. This simple approach should promise us a future large-scale synthesis of the patterned growth of the highly

well-aligned ZNs on various kinds of substrates buffered with a controlled morphology and roughness layer in an aqueous solution at low temperatures.

Acknowledgments

This work was financially supported by the National Science Council of the Republic of China, Taiwan under Contract No. NSC-92-2216-E-009-014.

References

(1) Hu, J.; Odom, T. W.; Lieber, C. M. *Acc. Chem. Res*. 1999, *32*, 435.

(2) Zamfirescu, M.; Kavokin, A.; Gil, B.; Malpuech, G.; Kaliteevski, M. *Phys. Rev. B*. 2002, *65*, 161205.

(3) Lieber, C. M.; Cui, Y. *Science* 2001, *291*, 851.

(4) Duan, X.; Huang, Y.; Cui, Y.; Wang, J.; Lieber, C. M. *Nature* 2001, *409*, 66.

(5) Park, W. I.; Yi, G.; Kim, M.; Pennycook, S. J. *Adv. Mater*. 2003, *15*, 526.

(6) Wu, Y.; Yang, P. J. *Am. Chem. Soc.* 2001, *123*, 3156.

(7) Chiou, W. T.; Wu, W. Y.; Ting, J. M. *Diam. Relat. Mater.* 2003, *12[10-11]*, 1841.

(8) Lee, C. J.; Lee, T. J.; Lyu, S. C.; Zhang, Y.; Ruh, H.; Lee, H. J. *Appl. Phys. Lett.* 2002, *19*, 3648.

(9) Vayssieres, L.; Keis, K. *J. Phys. Chem. B* 2001, *105,* 3350-3352

(10) Yamabi, S.; Imai, H. *J. Mater. Chem.* 2002, *12*, 3773

(11) Choy, J. H.; Jang, E. S. *Adv. Mater.* 2003, *15*, 1911

(12) Lin, C. C.; Hsiao, C. S.; Chen, S. Y.; Cheng, S. Y. *J. Electrochem. Soc.* 2004, in press.

(13) Bailar, J. C.; Emeleus, H. J.; Nyholm, R. and Trotman-Dickenson, A. F. Comprehensive inorganic chemistry, vol. 3. Pergamon Press, Oxford, 1975.

(14) Manna, L.; Scher, E. C.; Alivisatos, A. P. *J. Am. Chem. Soc.* 2000, *122*, 12700.

(15) Trentler, T. J; Hickman, K. M.; Goel, S. C.; Viano, A. M.; Gibbson, P. C.; Buhro, W. E. *Science* 1995, *270*, 1791.

(16) A. R. West, Basic solid state chemistry, pp. 244, John Wiley & Sons, 1999.

(17) C. C. Lin, H. P. Chen and S. Y. Chen, submitted to Adv. Mater. (2004).

(18) Liu, B.; Zeng, H. C. *J. Am. Chem. Soc.* 2003, *125*, 4430

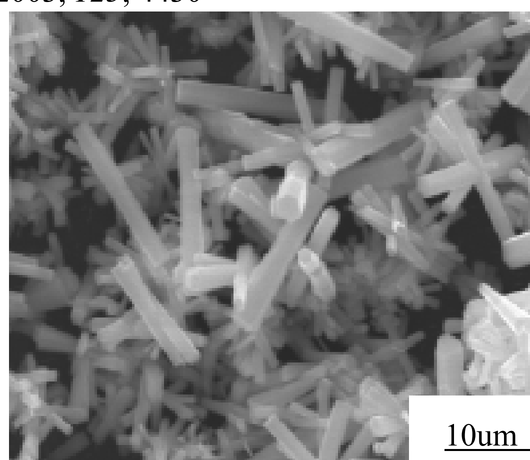

(a)

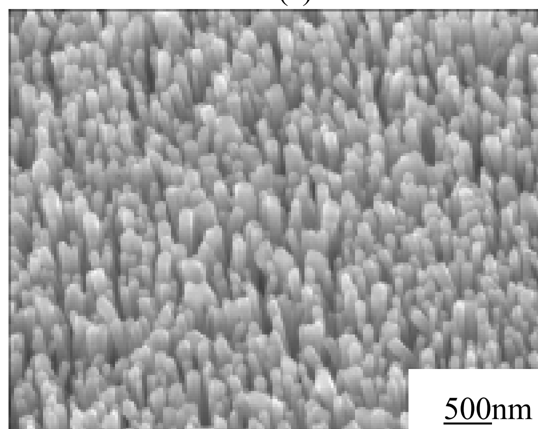

(b)

Fig. 1. SEM micrographs of ZnO nanorods grown on different substrates: (a) Si substrate and (b) ZnO_f/Si substrate.

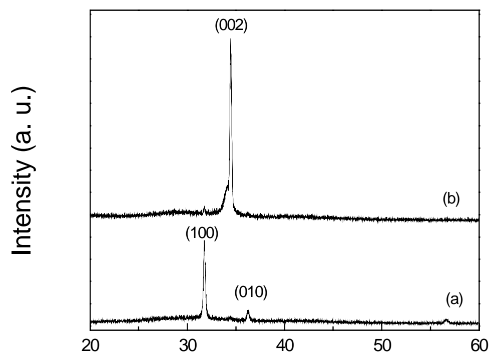

Figure 2. X-ray diffraction patterns of ZnO nanorods grown on (a) Si and (b) ZnO_f/Si substrates.

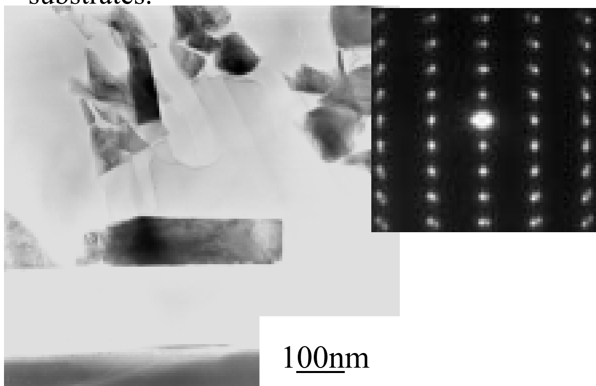

(a)

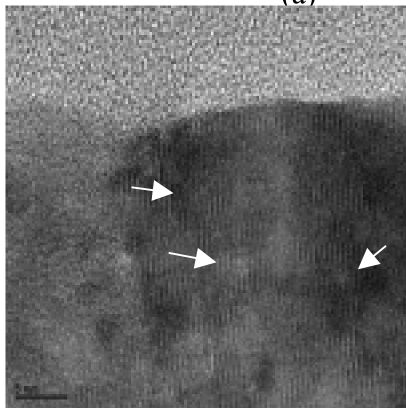

(c)

Figure 3. (a) TEM bright field (BF) image and (b) corresponding selected area diffraction pattern of ZnO nanorods grown on Si substrate. (c) Showing the lattice fringes of ZnO nanorods in (a).

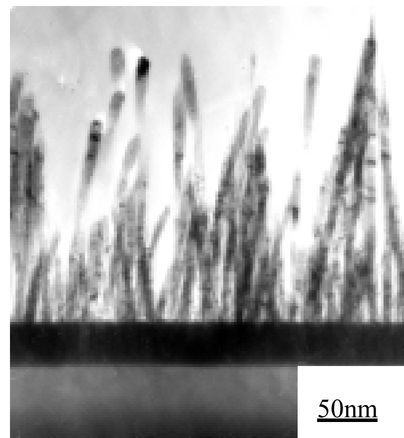

(a)

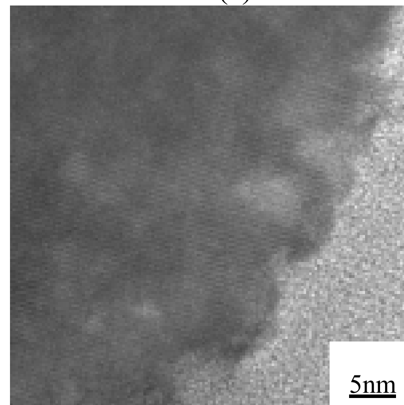

(b)

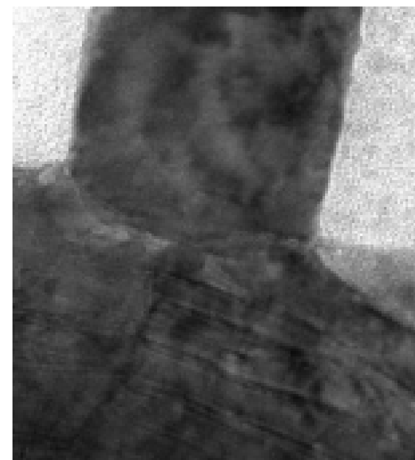

(c)

Figure 4 (a) TEM bright field (BF) image of aligned ZnO nanorods (ZNs) grown on ZnO_f/Si substrate. (b) High-resolution TEM images of the aligned ZNs and (c) the interface region between ZNs and ZnO_f/Si.

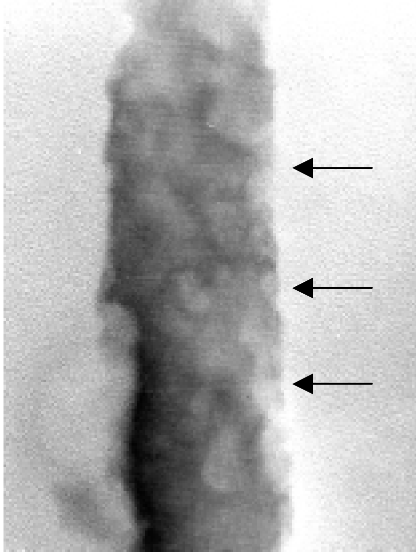

Figure 5. High-resolution TEM (HRTEM) image of ZnO nanorods showing the presence of stacking faults (SFs) as marked with arrows.

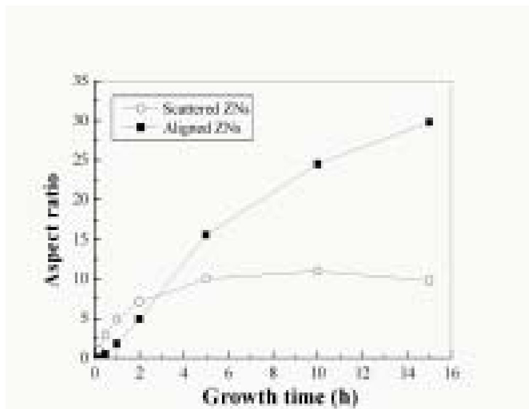

Figure 6. Dependence of aspect ratio (AR) on growth time for scattered and aligned ZnO nanorods.

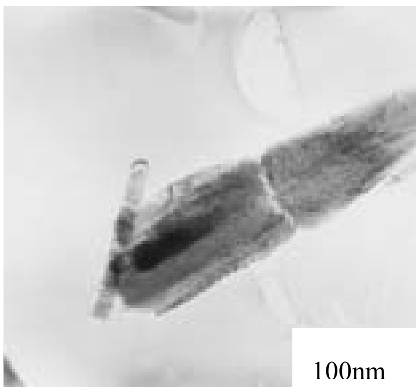

(a)

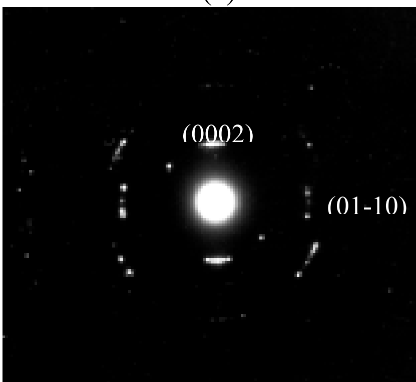

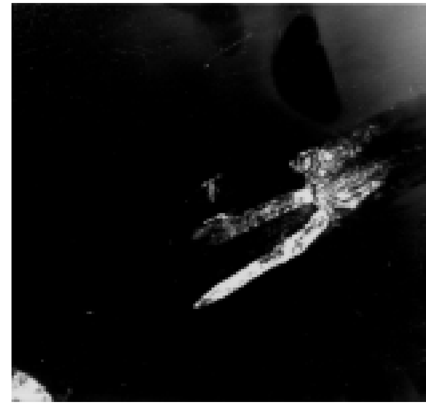

(c)

Figure 7. (a) TEM bright-field image, (b) corresponding selected area diffraction pattern and (c) dark-field image of self-assembled ZnO bundles.

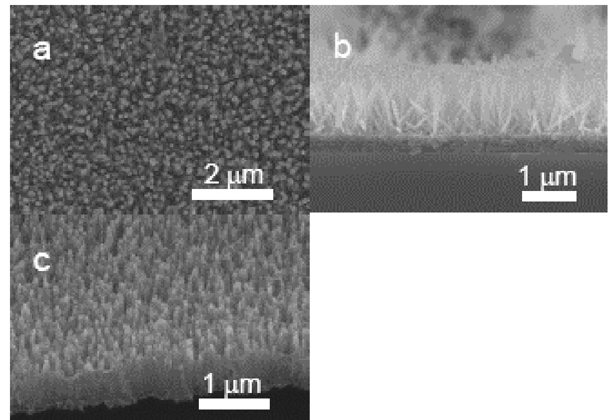

Figure 8. SEM images of large arrays of oriented ZnO nanorods grown on polystyrene (PS)/polycarbonate (PC) substrates for 8 h. (a) Low magnification, face-on view. (b) Cross-sectional SEM image of ZnO nanorods grown PS/PC substrates. (c) SEM image of ZnO nano.

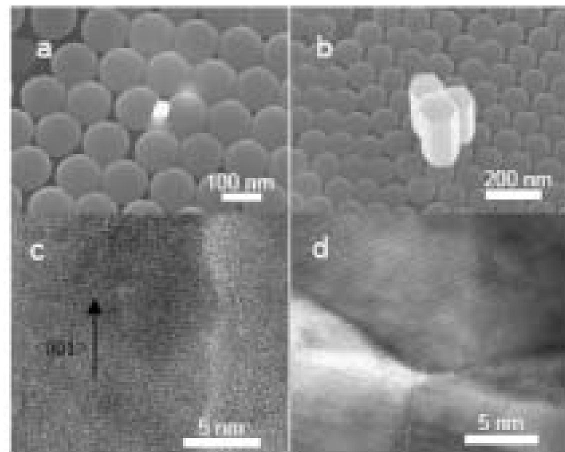

Figure 9. SEM images of ZnO nanorods grown on PS/PC substrates as a function of reaction time at 75 ℃. (a) 1h, and (b) 5 h. (c) High-resolution TEM image of ZnO nanorods grown on organic substrates. (e) High-resolution

TEM image of the interface region between ZnO nanorods and ultra-thin ZnO monolayer/PC.

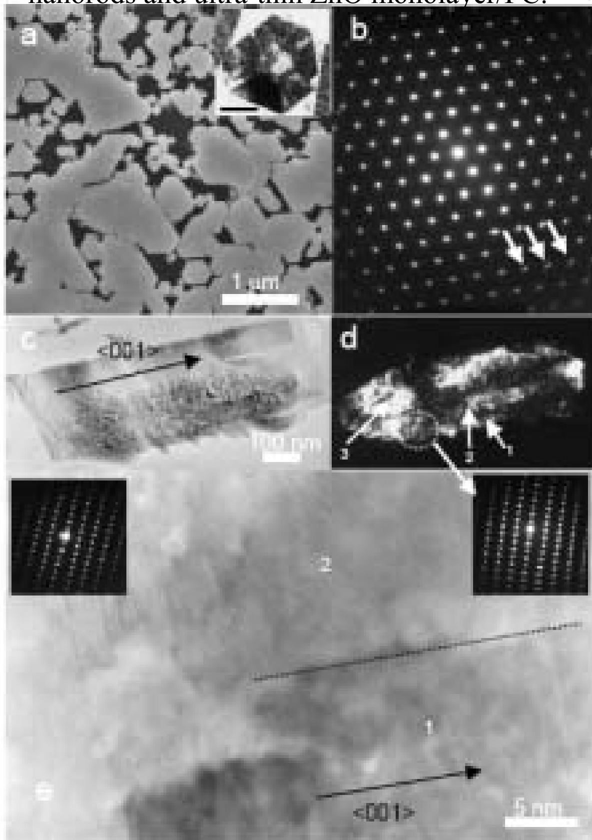

Figure 10. (a) Face-on view SEM image of well-aligned ZnO nanorods grown on PS/PC substrates for long-term growth (>24h). A <001> zone-axis TEM bright-field(BF) image of the coalescent ZnO nanorods (its scale bare is 100nm in the insert), and (b) a corresponding diffraction pattern for the inser of Fig. 3a. (c) Cross-sectional TEM (BF) and (d) dark-field (DF) images of the coalescent ZnO nanorods. (e) A high magnification BF TEM image of (c), showing the interface (marked with dash line) of the coalescent couple ZnO nanorods.

子計畫四:磊晶氧化鋅之製程及特性研究(2/3)

計畫主持人：張 立

計畫編號：92-2216-E-009-011-

參與人員：林智偉、吳佳玲

本年度計畫進行 CVD 鍍膜研究，化學氣相沉積系統(CVD)腔體內固定，量取適當前驅物 $Zn(C_5H_7O_2)_2$ 於氧化鋁坩堝內並放置系統中。在成長過程中，Si 基板溫度為 500℃，腔體壓力為一大氣壓。通入氮氣作為攜帶前驅物的氣體，前驅物的加熱溫度控制在 134℃。通入氧氣於腔體中進行反應，氧氣加熱溫度為 500℃。氮氣和氧氣流量均為 500ml/min。其中一部分在 Au/Si 基材上鍍具有高指向之 ZnO 膜，另外一部分在 Y2O3/Si(111)基材鍍上磊晶 ZnO，分別敘述如下。

一、在 Au/Si 基材上鍍具有高指向之 ZnO 膜

試片成長時間分別為 60 分鐘(試片 A)與 120 分鐘(試片 B)。XRD、SEM 與 TEM 結果顯示成長之氧化鋅結構具有良好的(0002)優選方向之柱狀結構

二、Y2O3/Si(111)基材

使用 CVD 和 PLD 方法鍍 ZnO 薄膜於 PLD 成長之 Y_2O_3/Si 基板上。穿透式電子顯微鏡(TEM) X 光繞射得知兩者方法成長的 ZnO 品質很接近，衔有磊晶之現象。

兩者都顯示出 ZnO 與 Y_2O_3 之間的晶體方向關係(orientation relationship)為 $\{0002\}_{ZnO}//\{111\}_{Y2O3}$，$\langle 0110\rangle_{ZnO}//\langle 112\rangle_{Y2O3}$，$\{11\bar{2}0\}_{ZnO}//\{440\}_{Y2O3}$ 。

子計畫五：

用晶圓接合與溼式蝕刻方式來剝離側向覆蓋生長之氮化鎵磊晶層 (2/3)

一、摘要

1. **中文摘要**

關鍵詞：氮化鎵，晶圓接合，異質磊晶，藍寶石，側向覆蓋生長。

本計畫主要的目的在於解決氮化鎵（GaN）薄膜異質磊晶（heteroepitaxial）於藍寶石（sapphire）基材所衍生的許多問題。期望藉由晶圓接合(wafer bonding)搭配濕式蝕刻(wet etching)於側向覆蓋生長磊晶片(ELOG GaN)上，轉移氮化鎵磊晶層於它種基板上。在前一年（第一年）的計畫中，我們發現由於在 ELOG GaN 上之遮罩層(mask)僅剩 300-500 埃（Å），蝕刻液很難有效的移除晶圓接合後的遮罩層。在這一年（第二年）的計畫中，我們先將 ELOG 上之遮罩層蝕刻後，在與晶圓接合，然後再移除藍寶石基材。此外，長在 GaAs 基板的 AlGaInP LED 結構，也被用來模擬轉移到 Cu 基板之效果。

2. **英文摘要**

Keywords：gallium nitride, sapphire, wafer bonding, heteroepitaxial, mask layer, epitaxial lateral overgrowth, epitaxy layer transfer.

This project was designed to solve the heteroepitaxial growth of GaN on the sapphire substrate. By selective wet etching of mask of the epitaxial lateral overgrowth (ELOG) GaN and bonding with other handle wafers, the ELOG GaN layers were transferred to handle wafers.

二 、前言及研究目的

氮化鎵具有優越的光電特性，且當其與氮化鋁（AlN）、氮化銦（InN）等化合物混合生長時可使能階由 2.0ev 連續改變至 6.3ev。幾乎涵蓋了所有可見光的範圍，造成近年產官學界均投入大量的資源進行相關的研究。然而，受限於熱力學需高溫高壓生長的先天限制，截至目前，大尺寸品質良好的氮化鎵塊材晶體，尚很難取得。因此目前商業用途的氮化鎵材料都是經由氣相沈積（vapor phase deposition）於非氮化鎵之氧化鋁基板上。但藍寶石本身的材料特性也使得氮化鎵材料的應用發展受到了限制，例如：

1. 藍寶石導熱性質不佳，元件容易產生 Joule heating 的效應，這不僅使元件效能變差，更使得元件的壽命與與可靠性減低。
2. 藍寶石本身是不導電的材料，使得兩電極之結構均必須鍍於元件作用層之上方。也正因基板不導電造成此元件之特殊結構，使得

製作氮化鎵發光二極體的過程必須多一道微影蝕刻的步驟，將氮化鎵磊晶層表面之部份 P 型區域去除，露出 N 型氮化鎵磊晶層，如此才可以於同一面同時獲得 P 型與 N 型氮化鎵之半導體表面。但由於氮化鎵具備半導體材料當中鍵結最強的離子性，相對於傳統的三五族半導體材料對於蝕刻液顯得較為鈍態，因此必須使用乾式的方式（如 ECR-RIE 與 ICP-RIE）進行氮化鎵的蝕刻製程，但使用乾式蝕刻氮化鎵還有光阻去除不易以及易損傷磊晶層品質等問題，進而影響元件的量產品質。由此可知，氮化鎵的不導電基板不僅增加元件製程複雜度並使得製造良率下降，還必須犧牲部分發光的作用層（active layer）供 N 型電極所用，降低了元件單位面積的發光亮度。

3. 製作氮化鎵發光二極體時，藍寶石基材必須有一定厚度（一般＞300μm）以避免因高溫而產生的變形。但因藍寶石的硬度過高（其莫氏硬度為 9），使得元件製作完成後不易進行 dicing，又因為藍寶石晶體對稱性的影響，造成使用傳統 dicing saw 的切割方式會損失較大面積的磊晶層，且切割刀具的磨損量也會增加並導致生產成本增加。切割過程中的藍寶石不規則崩裂也使我們無法得到想要的晶粒形狀，造成生產良率降低。
4. 由於藍寶石與氮化鎵晶格常數的不匹配和熱膨脹係數的差異極大，導致磊晶生長時氮化鎵薄膜的缺陷如差排、疊差等等…密度甚高。在藍寶石與氮化鎵界面處的差排（dislocation）密度常高達 $10^{10}cm^{-2}$ 以上，並且會延伸到元件結構之上。磊晶缺陷的存在容易使作用層失效並大幅的降低元件的特性。

透過晶圓接合技術，則可以將氮化鎵薄膜轉移到導電性和導熱性較佳的其他材料基板上。

本實驗室在在第一年的計畫中，發現由於在 ELOG GaN 上之遮罩層(mask)僅剩 300-500Å（原本為 1000Å），蝕刻液很難有效的移除晶圓接合後的遮罩層。在這一年的計畫中，利用長出未密合的 ELOG 的 GaN，將 ELOG 上之遮罩層蝕刻後，在與晶圓接合，然後再移除藍寶石基材。

此外，長在 GaAs 基板的 AlGaInP LED 結構，也被用來模擬轉移到 Cu 基板之效果。

三 、研究方法

在氮化鎵側向覆蓋成長法當中，會鍍覆數百至 1,000Å 的 SiO_2 遮罩層(mask) 。經由一般的 IC 蝕刻方式，蝕刻出條狀的遮罩層。在經由氣相沈積出未密合的 ELOG GaN。以上部分，是由廠商製造。我們將 ELOG 上之遮罩層蝕刻後，在與晶圓接合，然後再移除藍寶石基材。

由於現階段所得之 ELOG GaN 非發光的 LED 結構。為證明晶圓接合及轉移基板之效果。所以我們拿，長在 GaAs 基板的 AlGaInP LED 結構，轉移到 Cu 基板，來作模擬。其中， ITO 層被拿來當作 current-spreading 與中間接合介質。經過在無塵室清洗後，放在 Ar 氣氛中，在

400°C 至 600°C 接合 30 分鐘。

三 、結果與討論

1. ELO GaN 之晶圓接合及分離

在 SiO_x 的遮罩層移去後，ELO GaN 與 Cu 基板在 500 ~ 600°C 進行接合。冷卻後，於 Sapphire 基板上易有 crack 產生，如圖（一）所示。其原因可能是在冷卻時，Sapphire 與 Cu 之熱膨脹係數之差異(Sapphire= 7.5×10^{-6}/K；Cu = 16.8×10^{-6}/K) 而產生熱應力。施予適當之剪應力，可將基板分開。若先以淬火之方式增加薄膜間的應力，再加上適當之剪應力，可得到較佳之分離效果，如圖（二）所示。

最後，為了判斷 bonding 對薄膜之特性是否有影響，藉由 PL 光譜圖發現 bonding 前後之 FWHM 並無改變，但 bonding 後之試片有 blue shift 的現象產生，其原因可能為於氮化鎵結接合於銅基板，因降溫時氮化鎵薄膜之熱膨脹係數分別小於銅與藍寶石基板，而產生壓縮應力所致。

2. AlGaInP LED 結構轉移到 Cu 基板

我們發現，當溫度低於 400°C 時，樣品無法接合，溫度若高到 600°C的話，銅又會滲透 ITO 層，導致 LED 的結構遭到破壞。在 500°C下加熱 30 分鐘，銅尚不會穿透 ITO 層，而樣品又可以順利接合。轉移後的試片如圖（三）所示。由於銅具有較高的熱導率及較低的熱阻抗，因此散熱的效果較佳。如圖（四）所示，比起傳統的 GaAs 基板的 LED，銅基板 LED 的操作電流可以高達 800 mA，而其發光峰值強度可高達 1230 mcd。該系統於室溫下連續以 20 mA 的電流操作 500 個小時後，其發光強度衰減的幅度不到 5%。詳見我們在 Applied Physics Letters 發表之論文。[1]

三 、未來的方向

(1) 請合作的單位廠商提供 LED 或 LD 結構之 ELO GaN。

(2) Cu 基板之切割。

(3) 不同之導電/導熱基板，以利試片之切割。

四 、參考文獻

1. Wei Chih Peng and YewChung Sermon Wu, " High-power AlGaInP light-emitting diodes with metal substrates fabricated by wafer bonding," Appl. Phys. Lett. 84(2004) PP1841-1843.

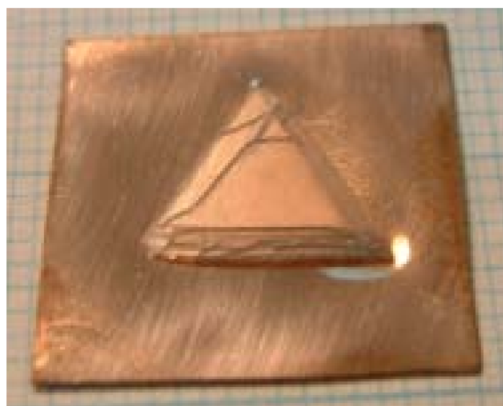

圖一 氮化鎵接合於銅基板上，冷卻後，Sapphire 基板上有 crack 產生。

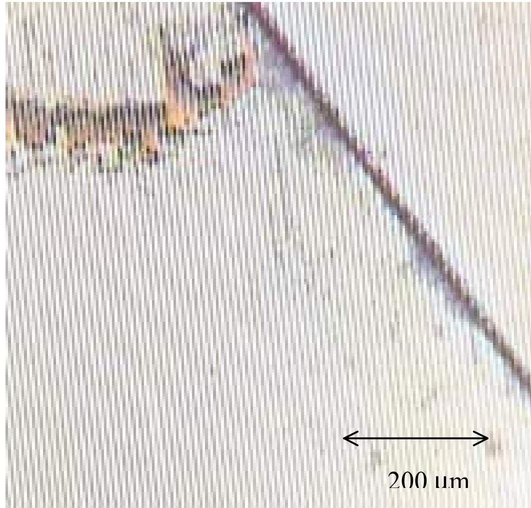

圖二 以淬火之方式再施予適當之剪應力之試片。

(a)

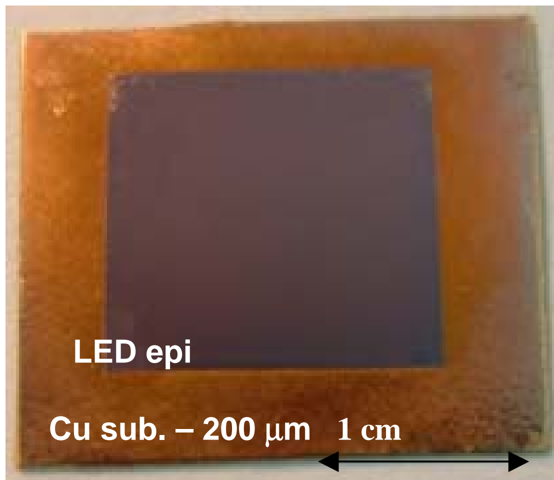

(b)

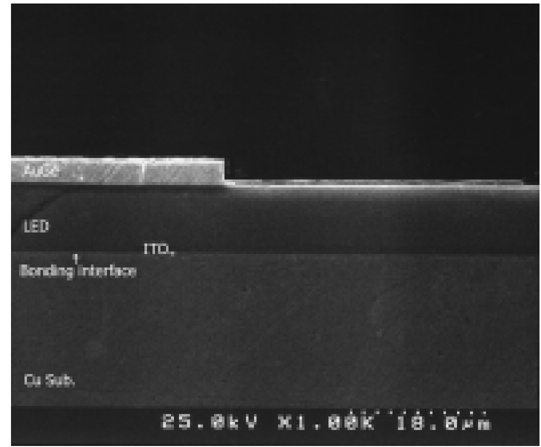

圖三 LED 接合在 Cu 基板上之(a)上視圖(b)剖面圖。

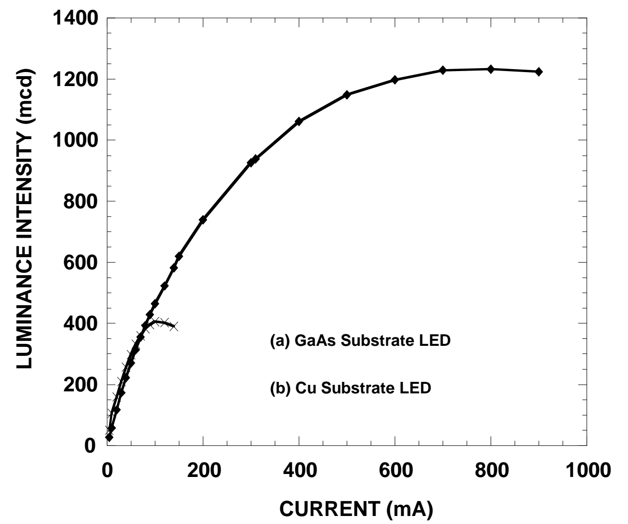

圖四 (a) GaAs Substrate LED 與(c) Cu Substrate LED 之 L-I 曲線

子計畫六：
光記錄媒體材料、性質及其應用於光碟記錄容量提升之研究(2/3)
A Study of Optical Recording Media, Properties and Their Applications to Increase the Storage Capacity of Optical Disks (2/3)

計畫編號：NSC92-2216-E009-013
執行期限：92/08/01 – 93/07/31
主持人：謝宗雍 國立交通大學 材料科學與工程學系 教授

一、 中文摘要

本年度之研究包含（1）GeInSbTe（GIST）光碟資料傳輸速度之提升與（2）$ZnO-SiO_2$ 微晶玻璃(Semiconductor-doped Glass, SDG)材料之開發。在光碟資料傳輸速度之提升部分，氮氣摻雜被應用於提昇非晶相-晶相的相變化速度。以氮氣摻雜來產生許多均勻分佈於記錄層的微小氮化物，而這些氮化物的存在則提供許多有利於非晶相-晶相間相變化的優選位子。當摻雜的氮氣/氬氣比率為 3%時，GeInSbTe 相變化記錄光碟在無嚴重損害訊號抖動(Jitter)值的情況下，其再結晶速率增加約 1.6 倍。微晶玻璃(SDG)部分，本計畫以貼靶濺鍍法在 SiO_2 中長成 5 至 10 nm 奈米分佈之 ZnO 微粒，PL 量測顯示貼靶面積增加至 20%、30%時，發光峰值約為 560 至 580 nm，符合 ZnO 的綠光轉換特性(Green Band Transition)，此能階主要為 ZnO 自身缺陷所形成；當低貼靶面積時的發光峰值則偏移至 470 nm。造成 ZnO 量子點的光譜峰值向短波長呈現不連續偏移的原因尚未明瞭，有待後續之研究探討 ZnO 量子點的量子侷限效應(Quantum Confinement)與結構缺陷對發光特性的影響。

關鍵詞：GeInSbTe 光碟、資料傳輸速度、$ZnO-SiO_2$ 微晶玻璃。

Abstract：This project of this year studies the enhancement of data transfer rate of GeInSbTe optical disk and the preparation of $ZnO-SiO_2$ SDG thin film. Nitrogen doping was applied to enhance the velocity of amorphous-crystalline phase transformation. The N_2 doping produced tiny nitride precipitates uniformly distributed in the recording layer and provided numerous preferential sites for phase transition. At the doping N_2/Ar ratio = 3%, the recrystallization velocity of GIST phase change recording media was increased up to 1.6 times without severely damaging the signal jitter values. In the part related to $ZnO-SiO_2$ SDG films, the emission peak measured by PL was about 560 ~ 580 nm (yellow) with the chip area coverage ratio of 20% and 30%. The emission was caused by the recombination of the carrier at the deep trap levels that are induced by the intrinsic defects of ZnO. However, the emission peak shifted to about 470 nm (blue) with low chip area ratio. The reason causing the un-continuous shift of the emission peak to shorter wavelength is unclear and future study is required.

Keyword: GeInSbTe optical disk, data transfer rate, $ZnO-SiO_2$ SDG thin film.

二、緣由與目的

數據資料之儲存與取用是當今資訊產品使用中的重要部份。現行資料之儲存可分為磁記錄與光記錄兩大類，光記錄通常以雷射光進行資料之記錄，是當今資料儲存最熱門、最重要的產品。

光碟研究的重要方向之一為提高資料傳輸速率，故相變化光記錄材料必須擁有更高的非晶相-晶相相變化速度。共晶系統的銻-碲(Sb-Te)合金亦或稱為快速成長型相變化合金最為大家所注目，因為此材料在短波長雷射及高數值孔徑的透鏡系統下擁有良好的訊號特性及較高的再結晶速率。本實驗以氮氣摻雜於相變化光碟的 GeInSbTe 記錄層中，並以動態測試機對其訊號特性及資料傳輸速率加以研究，而穿透式電子顯微鏡(TEM)則是被用來觀察氮氣摻雜對微結構所造成的影響，並且更進一步對微結構的變化與再結晶速率(或資料傳輸速率)做探討。

光碟的另一重要研究方向為提升紀錄密度，使用短波長、藍光雷射的讀寫頭為改善之方法之一[1]。目前所量產的藍光 LED 主要以 GaN 做為活性發光區，然而由於 GaN 缺乏良好晶格匹配的基板，加上氮化物的強化學穩定性使得微影蝕刻製程需以 RIE 進行，在形成 Ti/Al 歐姆接觸時容易形成 TiN 或 Al_2O_3 而造成電阻值的增加，加上 *p*-GaN 成長不易，因

此造成了 GaN 藍光 LED 在製程上的困難度[2-4]。ZnO 於近年來被視為最具有發展藍光 LED 潛力的材料之一，為直接能隙的半導體 E_g ~ 3.34 eV (與 GaN 相近, E_g ~ 3.32 eV)，熔點則高達 1975℃，可提高元件操作壽命及可靠度，本身亦可形成良好導電薄膜有利於歐姆接觸的製程，並可與一般酸反應進行濕式蝕刻，與 GaN 相比具有更有利的元件設計與製程彈性空間。ZnO 與 GaN 同樣具有壓電特性，且激子鍵結能(Exciton Binding Energy)高達 60 meV，具所謂的 Green Band Transition 特性(GaN 則為 Yellow Band Transition)，已有研究指出其發光特性機制與 GaN 極為相似，因此可望成為未來藍光 LED 新趨勢材料。

三、實驗方法

（1） 光碟資料傳輸速度研究部分：光碟試片在真空壓力低於 1×10^{-6} torr 的濺鍍系統製成，結構為 PC 基板/ZnS-SiO$_2$ (55 nm)/GIST-(N)$_x$ (16 nm)/ZnS-SiO$_2$ (11 nm)/Al-Cr (133 nm)，濺鍍記錄層時，不同氮氣摻雜的試片以氮氣/氬氣流量比例分別為 0%、0.5%、1%、3%、5%及 10%之條件製成，表 1 為各膜層的濺鍍條件及試片編號。光碟試片經初始化後，隨即以動態測試機進行訊號特性量測。TEM 的試片製作係先將 PC 基板研磨減薄，再以 3M 膠帶剝除反射層，最後再以二氯甲烷溶除剩餘的 PC 基板，並將試片置於銅網上後進行光碟 TEM 的微結構觀察。

（2） ZnO-SiO$_2$ 微晶玻璃部分：以貼靶濺鍍法沉積 ZnO/ SiO$_2$ 於 Si 晶片上，並改變貼靶面積，真空腔壓力約為 1 ~ 2×10^{-7} torr，氬氣流量 20 sccm，工作氣壓為 5×10^{-3} torr。並進行 ESCA、XANES、PL 量測與 TEM 觀察。

四、結果與討論

（1）**光碟資料傳輸速度研究**：表 2 為各試片之 8T 訊號的擦拭率與光碟線速度及其所對應之資料傳輸速率的關係圖。GIST 相變化碟片的擦拭率必須大於 25dB，才不致於在直接覆寫(DOW)的過程中發生問題。從表 2 中可發現，沒有氮氣摻雜的試片(N000)僅能通過低於線速度 5.3 m/sec 的擦拭率測試；有氮氣摻雜的試片(N030)則能通過線速度 8.8 m/sec 的擦拭率測試，故 N030 試片的再結晶速率大約為 N000 的 1.6 倍，故適量的氮氣摻雜有利於相變化光碟之再結晶速率(或資料傳輸速率)的提昇。圖 1 為試片 N000 與 N030 之訊號抖動值與直接覆寫次數的關係圖。由圖 1 可知，N000 與 N030 試片的訊號抖動值並無隨直接覆寫次數的增加而有明顯的差異，故少量的氮氣摻雜不會對光碟的訊號特性產生負面的影響。圖 2(a)及 2(b)分別顯示 N000 及 N030 試片於線速度 7 m/sec 與 10.5 m/sec 寫入之 8T 訊號的顯微結構。圖 2(a)及 2(b)中皆可發現常見於共晶合金系統的薄板狀結構，此外圖 2(b)中亦可觀察到許多微小的顆粒均勻分佈於試片 N030 的記錄層中，這些尺寸小於 10 nm 的微小顆粒可能為 Ge、Sb、Te 或 In 之氮化物，這些氮化物經雷射照射後亦能穩定存在。圖 2(c)及 2(d)分別為 N000 及 N030 試片的 8T 訊號於線速度 7 m/sec 與 10.5 m/sec 下進行擦拭後的顯微結構，其顯示沒有氮氣摻雜的試片(N000)經擦拭後仍存有殘餘記號，而經氮氣摻雜的試片(N030)則無殘餘的記號。

（2）**ZnO-SiO$_2$ 微晶玻璃之研究**：圖 3 為不同貼靶面積對濺鍍成分的 ESCA 分析結果。圖 4 則為 XANES 分析。ZnO 含量隨貼靶面積增加而有達到飽和現象，XANES 分析則得知以貼靶法濺鍍可成長以化合物態存在的 ZnO 顆粒。圖 5(a)、5(b)與 5(c)分別為貼靶面積 10、20、30%的 ZnO-SiO$_2$ 薄膜的 TEM 影像。當貼靶面積為 20%時，ZnO 顆粒的大小分布變得較不均勻，而貼靶面積為 30%時可見 ZnO 顆粒有明顯疊合現象。圖 6 為 PL 量測結果。650 nm 的高峰值為 He-Cd 325 nm 雷射的共振模態，其餘較銳利的高峰值為未完全過濾的雷射側模所造成的訊號，而較寬的才為 ZnO 的發光光譜。如此寬的發光波長與 ZnO 的 Deep Trap 發光機制有關，明顯可見低貼靶面積的發光波峰約為 470 nm (近藍光)較高貼靶面積的峰值 550 ~ 580 nm (近黃光)偏移了近 100 nm，相對於其發光能階應有近 0.5 eV 的能量差。造成如此的發光機制原因尚不明確，但應與 ZnO 顆粒所形成的量子效應或與形成量子點結構而造成的 Defect Level 有關。

五、計畫成果自評

本年度計畫共完成光碟資料傳輸速度之提升研究與 ZnO-SiO$_2$ 微晶玻璃之製備與光學性質量測研究。光碟資料傳輸速度之研究部分我們發現適量的氮氣摻雜可以將 GIST 光碟的資料傳輸速度提升 1.6 倍，此部分成果除發表於 2004 年 ODS Conference，亦已投稿於 *Jap. J. Appl. Phys.*。ZnO-SiO$_2$ 微晶玻璃則成功地在

SiO_2 薄膜中製成奈米尺度的 ZnO 顆粒，PL 光譜糧測發現其似有在藍光波長份範圍發光之可能，目前正加緊研究，如能成功，對能提升光碟紀錄密度之藍光 LED 關鍵元件將有所貢獻。

六、參考文獻

[1] A.B. Marchant, "*Optical Recording – A Technical Review*", Addison-Wesley, (1990).

[2] D. C. Reynolds, *et al*., *J. Solid State Communications*, **101**(1997), No. 9, p.643.

[3] A. van Dijiken, *et al*., *J. Lumi*., **87**-**89**(2000), p.454; *ibid*, **90**(2000), p.123; *ibid*, **92**(2001), p.323.

[4] X. T. Zhang, *et al*, *J. Lumi*., **99**(2002), p.149.

表 1、 光碟膜層的濺鍍條件及試片編號。

試片編號	N_2/ Ar 流量比	靶材種類	濺鍍壓力 (m Torr)	濺鍍功率(W)
	0	ZnS-SiO_2	3	250 (RF)
	0	Al-Cr	3	400 (DC)
N000	0	GeInSbTe	3	50 (RF)
N005	0.5%	GeInSbTe	3	50 (RF)
N010	1.0%	GeInSbTe	3	50 (RF)
N030	3.0%	GeInSbTe	3	50 (RF)
N050	5.0%	GeInSbTe	3	50 (RF)
N100	10.0%	GeInSbTe	3	50 (RF)

表 2、光碟試片於不同線速度下的擦拭率。

傳輸速率 (Mbps)	11.08	16.62	22.16	27.70	33.24
線速度(m/sec)	3.5	5.3	7.0	8.8	10.5
試片	DC 擦拭率				
N000	39.89	28.03	12.38*	---	---
N005	48.59	43.86	34.36	16.58*	---
N010	37.17	48.81	42.00	17.28*	---
N030	36.75	40.36	42.34	26.00	16.91*
N050	×	×	×	×	×
N100	×	×	×	×	×

*不能擦拭　　╳不通過動態試驗

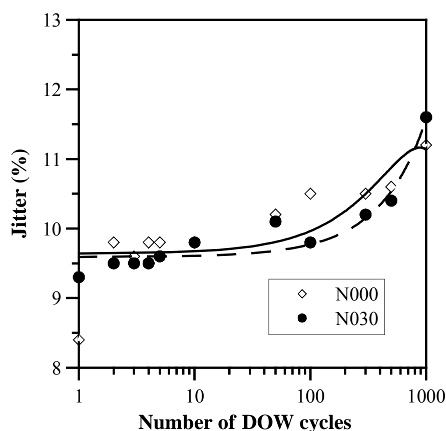

圖 1、N000 與 N030 試片之訊號抖動值與直接覆寫次數的關係圖。

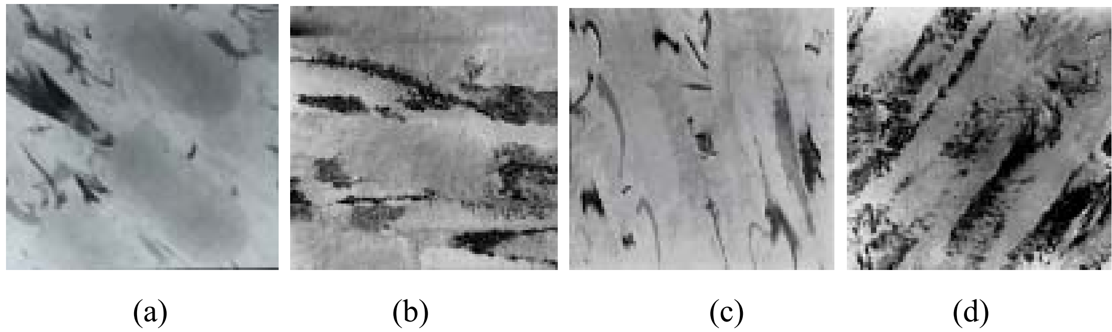

(a) (b) (c) (d)

圖 2、(a)N000 及(b)N030 試片分別於線速度 7 m/sec 與 10.5 m/sec 所寫入之 8T 訊號。(c)N000 及(d)N030 試片分別於線速度 7 m/sec 與 10.5 m/sec 下進行 8T 訊號擦拭後的顯微結構。

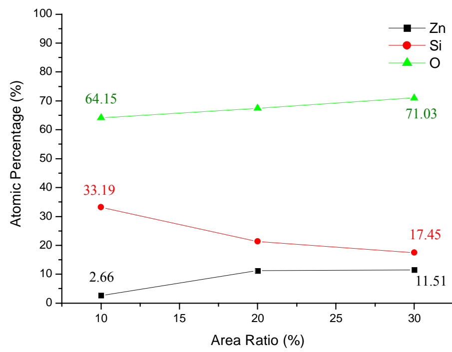

圖 3、試片成分對貼把面積的 ESCA 分析。

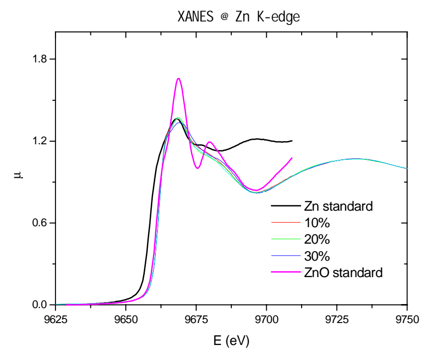

圖 4、XANES 分析。

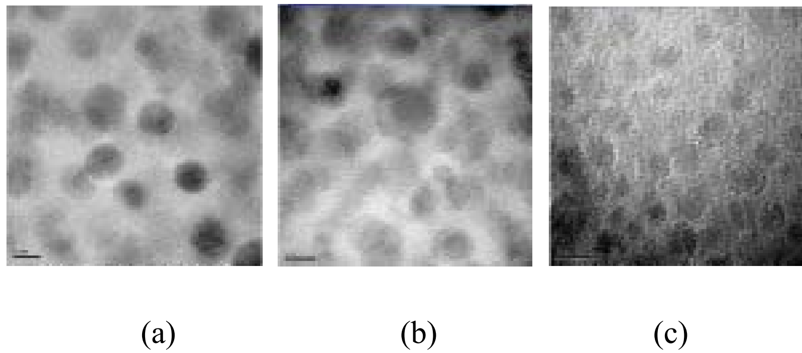

(a) (b) (c)

圖 5、ZnO-SiO_2 薄膜的 TEM 影像，貼靶面積分別為(a) 10% (b)20% (c) 30%。

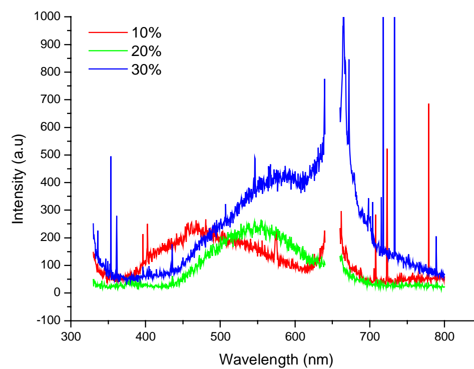

圖 6、PL 量測結果。